AIAA JOURNAL
Vol. 39, No. 2, February 2001

Lateral Buckling Behavior of Pneumatically Stiffened, Reinforced Composite Beams in Bending

William A. J. Higgs,* Liyong Tong,† and Grant P. Steven‡
University of Sydney, Sydney, New South Wales 2006, Australia

The use of inflatable structures has often been proposed for aerospace applications. The advantages of such structures include low weight, easy assembly, and storage. The aim of this study is to investigate the effects of finite inflation on the subsequent buckling response of a carbon-fiber-reinforced composite beam (RCB) in bending. A finite element solution for three incremental beam configurations is developed. The first lateral buckling mode is used to determine the structural efficacy of the inflated beam. For each beam, the bending moment required to induce lateral buckling was determined. A nonlinear material and geometrically nonlinear finite element solution is obtained for the inflation load. A Rik method solution was then obtained to examine the postbuckling response of the RCBs. In addition, an eigenvalue extraction was performed to study the intrinsic influence of air pressure on the structural stability of RCBs. Finally, experimental data were obtained to verify the theoretical results. It is found that a simple eigenvalue extraction provides a conservative estimate of the critical buckling moment for preliminary design purposes. Furthermore, there is good correlation between theory and experiment and there exists noticeable interaction between the beam and pressurized air prior to final buckling for this type of reinforced composite beam.

I. Introduction

PNEUMATIC or inflated structures, which depend on internal pressure for form and function, have received considerable attention in aerospace research.[1,2] Automatic assembly, minimal storage, and lightness make inflatable structures most suitable for applications such as satellites and space stations.[3–5] Frequently, these structures are formed of fabric, sewn into a closed tube, and, when inflated, result in a structural cylindrical beam. The ease of fabrication and ability to span distances and carry loads in this structural form make the inflated cylinder the natural pneumatic analog to the elastic beam.

For all applications, information is required on the load-carrying capabilities of this type of inflatable structure. The design of inflated structures has generally been contrasted to the design of metal structures; the major difference is the nonlinear properties of the constituent materials and determination of the stability of the inflated structure.[2]

In the past, a structural analysis of inflated beams has been undertaken by using a number of strategies. Simple methods of analysis have been utilized to determine collapse loads for certain types of inflated structures,[6,7] such as inflatable reentry vehicles. Linear theory has been used for the structural analysis of inflatable plates[8] and has been verified experimentally.[9] However, the limitation of this theory is that it only applies when the internal pressure and applied loads are such that the structure's wall remains in tension.[1] Most of the applications for inflatable structures are not limited to this type of condition.

Frequent references have dealt with the examination of buckling of inflated circular beams acting as cantilevers. Linear shell analyses have been used to determine the collapse load of these inflated cantilever structures, on the assumption that at failure the root folds like a plastic hinge.[1,2,10] A relationship has also been established between beam curvature and moment for an inflated circular cylinder carrying a constant moment.[11] The buckling of inflated circular shells of appreciable wall thickness has also been analyzed and shows that buckling occurs as soon as the stress in the structure's wall becomes compressive.[12,13] Incipient buckling begins at a load for which the bending stress just cancels the axial stress due to pressure.[1] It has been shown that as the load increases beyond this value, the tube wall becomes slack in an axial direction over an increasing area. When the slackness extends completely around the root cross section, collapse takes place. The flexural stiffness of an inflated beam, in contrast, is independent of the pressure, provided that the pressure is large enough to prevent wrinkling of the beam and that the yield strength is not exceeded.[10] Improvement in the understanding of the problem of bending of inflated beams has been provided with use of the theory of "small deformations superimposed on large ones." This theory accounts for the changing geometry and changing material properties that occur during inflation; linear elasticity is incapable of accounting for these changes.[14] Variational methods have been used with shell models of inflated beams to determine beam deflection under a variety of loads.[15] In a classical study, Comer and Levy[3] modeled the behavior of an inflated cantilever beam between incipient buckling and final collapse in a manner similar to beam to conventional beam theory. Their solution resulted in an expression of the problem in terms of two-dimensional variables, which when solved gave the beam deflections. The model was reformulated[16] to make use of the stress resultants instead of stress and an expression of the fabric moduli in terms of force per unit width to make the theory more applicable to fabric structures. Two papers[5,16] used a classical solution to find the deflections and stresses under bending based upon conventional beam theory with an assumed stress distribution in the beam. Gosling and Riches[17] investigated further the load-deflection behavior of inflated beams by formulating triangular elements with a dynamic relaxation algorithm to solve for the displacements and stresses. In order to verify the numerical model presented, the same analysis was performed by utilizing the finite element method. The results of both analyses were in excellent agreement: a 1% difference for each of the 10 load cases performed.

In contrast to the case of a fabric cantilever beam, numerical solutions for the specific case of a reinforced inflatable composite beam in bending have not been investigated previously. This application of inflatable structures deserves due consideration. In light of the excellent accuracy afforded by the finite element method to provide solutions for displacement, stress, and collapse of inflatable structures, in general, we have performed a finite element solution for inflation and bending of this special case of an inflatable reinforced composite beam (RCB).

II. Experimental Investigation

A. Specimen Preparation

Pneumatically stiffened, composite-reinforced beams were fabricated from rubber[18] and reinforced with laminates of carbon fiber[19]

Received 14 July 1999; revision received 7 April 2000; accepted for publication 28 June 2000.

*Professor, Department of Aeronautical Engineering.
†Associate Professor, Department of Aeronautical Engineering; ltong@aero.usyd.edu.au. Senior Member AIAA.
‡Professor, Department of Aeronautical Engineering.

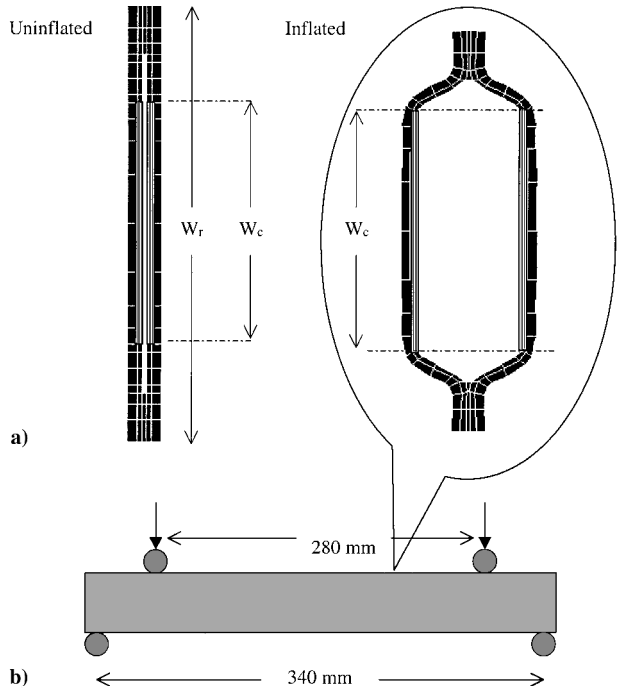

Fig. 1 Schematic of a) uninflated and inflated RCBs; dimensions W_c and W_r are defined in Table 4; and b) four-point bending setup, the same for all RCB configurations.

in a one-step (co-curing) process. Rubber provides the beam with the potential to expand radially and support higher bending loads with stiffening from the composite reinforcement.

Beams were prepared from two equal lengths of rubber sheet; each sheet was bonded on one side with three plies of carbon/epoxy tape. A Teflon "release" ply is placed on top of one of the rubber sheets, leaving 6 mm at the edges to permit rubber–rubber bonding and thereby provide an airtight seal. The Teflon release ply prevents the two sheets of rubber from curing together. The two reinforced rubber sheets are placed one on top of each other, vacuum bagged, and cured under temperature (175°C) and pressure (100 psi) in an autoclave for 2 h. After curing, the Teflon release ply is removed and two plugs are adhesively bonded in each end of the beam. For the beam to be pressurized with air, a hole is tapped into one end through which pressurized air can flow. The final configuration is shown in Fig. 1.

In this study, three configurations of composite-reinforced beams were tested with the purpose of examining the effects of increasing the second moment of area on the stability of the RCB. Beams were configured with increasing widths of reinforcing composite laminates, ranging from 20 to 30 mm in steps of 5 mm (W_c). To incorporate the reinforcing material, the dimensions of each supporting membrane rubber sheet was 40, 45, and 50 mm, respectively (W_r). All three configurations were of equal length to standardize this dimension for experimental bending tests. The Teflon sheet was dimensioned such that it gave a 6-mm bonded edge. The three beam configurations are labeled S20, S25, and S30, in increasing widths. Three beams of each configuration were fabricated for mechanical testing, for a total of nine RCBs.

Airpad rubber[18] was selected as the inflatable membrane material because it has the ability to bond to epoxy and itself under the prescribed conditions of temperature and pressure. This type of material is used frequently for aerospace applications, acting as a pressure intensifier for curing thick laminates of carbon fiber. The composite material used in the fabrication of the reinforcing structure is a Hexcel structural unidirectional carbon fiber (T300), impregnated resin (F263) laminate.[19] The material properties of both constituent materials are listed in Tables 1 and 2.

Each RCB was conditioned for approximately 50 inflation cycles prior to mechanical testing. Conditioning was performed to examine the integrity of the beam under repeated inflation pressure and to ensure that each RCB expanded into its fully developed state. In some cases, air leaks developed at discrete locations of the edges of the RCBs, and these were removed from the study. This type of leak developed in the early stages of development and was eliminated subsequently by increasing the autoclave cure pressure. Only those RCBs that could sustain cyclic pressurization for 50 cycles were included in the mechanical testing study.

Table 1 Orthotropic properties for unidirectional composite material (MPa)

E_{11}	E_{22}	E_{33}	ν_{12}	ν_{13}	ν_{23}	G_{12}	G_{13}	G_{23}
1.22e5	8760	8760	0.27	0.27	0.26	3563	3563	2860

Table 2 Airpad rubber properties; Ogden polynomial $N = 1$

μ_1	α_1
1.436 MPa	2.182

B. Testing Setup and Procedure

The RCBs were testing in four-point bending by using a custom fabricated load train as schematically shown in Fig. 1. The load train consisted of two pairs of rollers that are free to rotate. An Instron materials testing machine applies an equal and opposite torque to each pair of rollers to generate a constant bending moment between the two inner rollers. Bending was performed at a crosshead rate of 5 mm/min. During the loading process, the deflection of the rollers and load magnitude were recorded.

Each RCB was inflated to the required pressure and tested in bending. A pressure gauge recorded inflation pressure throughout each test. During initial loading, care was taken to ensure that the RCB did not displace laterally or twist between the rollers as a result of the action of misalignment alone. The test was considered complete when one of three events took place: 1) the beam buckled, 2) the beam mechanically failed, or 3) an air leak developed.

Each configuration of RCB was tested three times, for a total of 27 tests.

C. Experimental Results

The desired outcome of the bending test was to determine the maximum buckling moment and the associated buckling mode for a given inflation pressure and RCB configuration. The bending tests produced both of these characteristics for each RCB configuration.

It was observed that all beams failed by either local or global first-mode lateral buckling. In the small amount of cases in which local buckling took place, it occurred in the form of a pronounced lateral displacement or bulging of one side of the RCB, located closest to the inner rollers. This represented a minor instability, perhaps attributed to a slight rotational torque applied to the specimen. Additionally, this observation may indicate that the RCB structure is sensitive to slight imperfections in fabrication. This imperfection could arise during manufacture, could be attributed solely to small alignment errors, or both.

In 90% of the cases, a characteristic first mode of lateral buckling was observed (Fig. 2). The transition from the normal to the buckled shape was rapid and represented by a small drop in load. Following the small drop in load, the beam exhibited a moderate postbuckling stiffness. This postbuckling stiffness was directly dependent on the degree of rotational restraint in the region of the rollers. After the test was repeated a second and third time, each RCB demonstrated repeatability, which suggested that no material yielding took place during the buckling stage of testing. The buckling results are listed in Table 3 and demonstrate an increasing critical buckling load with the RCB size.

III. Numerical Modeling

A. Finite Element Models

The finite element method was chosen as the numerical technique because it is the most developed and offers the best tool for analyzing a nonlinear structure. A finite element software package, ABAQUS,[20] which is capable of analyzing nonlinear material and

Table 3 Maximum bending moment (N ·m) at the moment of lateral buckling

RCB type	Eigenvalue results (no air)	Nonlinear results (with air)	Measured
S20	2.84	3.29	4.89 ± 0.82
S25	4.16	5.10	6.17 ± 0.76
S30	5.32	6.85	7.43 ± 0.58

Table 4 Specimen configuration and FEA models

RCB type	FEA elements	FEA nodes	Laminate configuration	RCB length, mm	Composite width W_c, mm	Rubber width W_r, mm
Type S20	11,449	12,235	0/0/90 deg	280	20	40
Type S25	11,449	12,235	0/0/90 deg	280	25	45
Type S30	11,449	12,235	0/0/90 deg	280	30	50

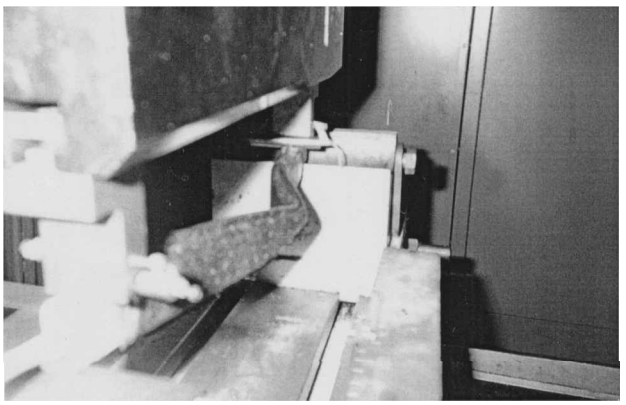

Fig. 2 Experimental first lateral buckling mode for a typical RCB.

geometrically nonlinear structures and is capable of modeling the pneumatic stiffness of the pressurized air on the structure, was utilized.

Three RCB configurations have been modeled and are described in Table 4. Each configuration of RCB is 280 mm in length, with noninflated widths of 40 mm for configuration S20, 45 mm for configuration S25, and 50 mm for configuration S30. The thickness of the rubber sheeting used to fabricate the RCB is 1.57 mm. At the edges, where the two sheets meet to form an adhesive airtight bond, the thickness is doubled.

The three-dimensional geometry has been carefully modeled in PATRAN[21] to reproduce the exact RCB dimensions. Three models representing each of the RCB configurations were generated.

In all RCB configurations a lay-up of 0/0/90 deg was modeled as solid composite hexahedral elements (C3D8). The orientation of the constituent orthotropic plies was such that the 0-deg ply is directed in the longitudinal direction of the beam with the normal directed toward the exterior of the RCB. Solid composite elements were attached to hyperelastic formulated C3D8H hexahedral elements, representing the rubber membrane. As described earlier, under set conditions of temperature and pressure, an adhesive bond is formed between the rubber and carbon fiber, and as such this joint was modeled as perfectly bonded in the analysis.

It is numerically inefficient to model the composite as a solid element given the physical dimensions of the laminate. However, three-dimensional F3D4 hydrostatic fluid elements have been incorporated into the model to represent the pressurized air and can only be represented as shell elements. This overrepresentation was deemed necessary.

Topologically, the hydrostatic fluid elements are surface elements, which cover the internal boundary of the RCB. Because the fluid elements have four nodes, there will be an additional constraint applied to the model. And because of the reduction in freedom, the analysis is limited to eight-node brick elements (C3D8), which would otherwise be expected to make the structure slightly stiffer than usual, so a dense mesh is used. Additionally, for the pneumatic fluid to be represented, a reference density, ambient pressure, and room temperature are necessary to satisfy the ideal gas model:

$$\rho = CP/(\theta - \theta^Z) \tag{1}$$

where ρ is the fluid density, P is the total fluid pressure, θ is the temperature, θ^Z is the absolute zero on the temperature scale being used, and C is a constant (0.00525 kg K/m). For this analysis, absolute zero is -273.16 K, ambient pressure is 0.10136 MPa, ambient temperature is 27°C, and air density is taken as 1.774 kg/m^3.

B. Modeling

Model solutions were performed by using ABAQUS,[20] and material models defined in ABAQUS were used. Epoxy material, representing the plugs, was assumed to be linear with Young's modulus of 4.0 GPa and Poisson's ratio of 0.31. The material model that best represented the incompressibility of the Airpad rubber[18] material was the general hyperelastic material model using a first-order Ogden strain energy potential. The form of this potential is

$$U = \sum_{i=1}^{N} \frac{2\mu_i}{\alpha_i^2}\left(\bar{\lambda}_1^{-\alpha i} + \bar{\lambda}_2^{-\alpha i} + \bar{\lambda}_3^{\alpha i} - 3\right) + \sum_{i=1}^{N} \frac{1}{D_i}(J_{el} - 1)^{2i} \tag{2}$$

where

$$\bar{\lambda}_i = J^{\frac{-1}{3}}\lambda_i, \lambda_i \tag{3}$$

are the principal stretches and J is the volume ratio, and λ_i are the stretches in the three orthogonal directions. The constants μ_i and α_i describe the shear behavior of the material and D_i the compressibility.

An ABAQUS input program was coded to determine the hyperelastic material constants. The test data were specified as nominal-stress, nominal-strain data. Uniaxial stress–strain data were obtained from uniaxial tests performed at 450 mm/min on standard dumbbell specimens. For each stress–strain pair, an equation was developed for the stress in terms of the strain invariants and the unknown hyperelastic constants, assuming incompressibility.

For the uniaxial case, the nominal stress T_U is

$$T_U = \frac{\partial U}{\partial \lambda_U} = 2\left(1 - \lambda_U^{-3}\right)\left(\lambda_U \frac{\partial U}{\partial \bar{I}_1} + \frac{\partial U}{\partial \bar{I}_2}\right) \tag{4}$$

where U is the strain energy potential, λ_U is the stretch in the uniaxial direction and I_i are the deviatoric strain invariants. If the Mooney–Rivlin form ($N = 1$) of the polynomial strain energy potential is used, then

$$U = C_{10}(\bar{I}_1 - 3) + C_{01}(\bar{I}_2 - 3) \tag{5}$$

and thus

$$T_U = \frac{\partial U}{\partial \lambda_U} = 2\left(1 - \lambda_U^{-3}\right)(C_{10}\lambda_U + C_{01}) \tag{6}$$

The polynomial potential is linear in the coefficients C_{ij}. Therefore a linear least-squares procedure was used. The Ogden potential is linear in the coefficients μ_i but strongly nonlinear in the exponents α_i. A nonlinear least-squares procedure similar to that of Ogden[22] is coded to determine μ_i and α_i simultaneously. Upon derivation of a set of constants, a material stability checks along the primary deformation modes, using the Drucker stability criterion.[23]

When deciding on the most appropriate hyperelastic model, both the Mooney–Rivlin ($N = 1, 2$) and Ogden models ($N = 1$–6) were fitted to the experimental uniaxial data. The Ogden model ($N = 1$) showed greatest correlation with the original stress–strain data and was selected as the hyperelastic material properties. The calculated Ogden $N = 1$ hyperelastic material properties are $\mu_1 = 1.4355$ MPa, $\alpha_1 = 2.182$ MPa, and because the material is incompressible, $D_1 = 0$.

The composite material used in the analysis is a Hexcel structural unidirectional carbon fiber (T300) impregnated with epoxy resin (F263). This composite is defined within ABAQUS as an orthotropic material with the properties listed in Table 1.

The independent elastic material properties E_1, E_2, G_{12}, and ν_{12} required for the three-dimensional lamina analysis were provided from manufacturer data. In the absence of experimental data for these properties, the assumption of transverse isotropy in the two-three plane was reasonable. The validity of this assumption has been demonstrated by experimental data available in the general literature.[24–26] The assumption of transverse isotropy implies

$$E_1 = E_2, \qquad G_{13} = G_{12}, \qquad \nu_{13} = \nu_{12}$$
$$G_{23} = E_2/2(1 + \nu_{23}) \tag{7}$$

Even with this simplifying assumption, ν_{23} must be measured or estimated for full knowledge of the nine independent elastic material properties. The need for all nine independent elastic constants, however, does not imply that the three-dimensional analysis will be sensitive to the choice of the through-thickness material property. For instance, a choice of ν_{23} of 0.5 vs 0.40 (a 20% difference) may only result in a 2% difference in the stress or strain results from a laminate or structural analysis.[27] Likewise, the use of a linear analysis when certain material properties are extremely nonlinear (i.e., in-plane and through-thickness shear modulus) may not affect laminate or structural analysis, and this too should be considered in a three-dimensional analysis.[27]

C. Loads and Boundary Conditions

A finite element solution was obtained for two load cases. The first load case inflates the RCB to a specified internal pressure. The pressurized air is represented as a compressible "pneumatic" fluid satisfying the ideal gas law. The pressurized air is modeled to investigate the coupling between the deformation of the RCB and the pressure exerted by the contained air on the RCB structure. It was anticipated that there would be some coupling between the rubber membrane and the pressurized air, reaching a maximum during collapse. This interaction is similar to the squeezing of a balloon; that is, squeezing the balloon in one direction will result in a bulge in the other.

This load is applied by specifying an internal pressure to one node representing the air cavity. Prior to the onset of instability, this is equivalent to applying a uniform pressure, representing the resultant hydrostatic pressure, to the internal boundary of the RCB. The volume is automatically adjusted to fill the internal boundary of the RCB. That is, air is assumed to enter and leave the cavity as needed to maintain the prescribed pressure. Prior to the application of the second load case, the internal boundary is sealed with the current air volume.

In the fabrication of the RCBs, a plug was placed in each end. One plug was tapped to permit airflow and subsequent pressurization. This had to be adequately modeled in the finite element analysis because stresses are developed in the RCB as a result of the plugging step of the fabrication process. Hexahedral elements (C3D8) were incorporated in the model to represent these plugs. During the inflation load case, these elements were deactivated and tied to adjacent displacing elements. Prior to load case two, these elements were reactivated in a strain-free state.

The second load case applies a couple to each end of the RCB to provide a typical four-point bending. As pure couples cannot be applied directly, the inner rollers were modeled as distributed forces acting across the transverse direction of the RCB. The outer rollers were constrained to permit movement only in the longitudinal direction of the beam. The RCB was constrained in such a manner to restrict torsional rotation at the inner and outer rollers. The level of constraint is equivalent to the experimental testing discussed earlier. As will be discussed in detail later, only an initial value for the applied couple has to be specified initially. It is recommended that this initial value represent some 10% of the anticipated maximum load. For example, for RCB type S30, the experimental maximum buckling moment was approximately 7 N · m applied at each end. Accordingly, an initial bending couple of 0.07 N · m was specified. The solution will then be sufficiently developed prior to the initiation of buckling. Solutions will be therefore developed around the region of buckling.

D. Solution Procedures

The first phase of the analysis is a geometric and material nonlinear analysis of the RCB to solve for the inflation loading only. In the nonlinear analysis the applied load is divided into increments. The solution starts with a small load increment, ΔP, and uses the structure's tangent stiffness, K_0, which is based on its configuration at u_0 and ΔP to calculate a displacement correction, c_a. With the use of c_a, the structure's configuration is updated to u_a. The Newton method is applied and often takes several iterations for each increment to determine an acceptable solution. At each increment the structure must be in equilibrium, and the net force acting at every node must be zero.

In the second phase an eigenvalue extraction is performed for the inflated shape obtained in the first phase of the analysis. The inflated displacements, material properties, and preloading were used as the initial state for the eigenvalue estimation. The linear buckling loads and modes are determined in this phase with the condition that air does not contribute to the stiffness of the RCB.

The third phase of the analysis comprises a nonlinear load-displacement analysis utilizing the modified Rik method[20] to determine the buckling bending load. When considering the geometric nonlinearity, the Rik method provides a load-displacement analysis to determine the collapse load. It was determined a priori that the postbuckling behavior of the RCB maybe either stable or unstable during part of the loading history, and the modified Rik method was selected to adequately handle this scenario. In this respect, a solution is developed around the point of collapse, so it is not necessary to specify a bending couple directly.

The solution load magnitude is defined according to

$$P_{\text{total}} = P_0 + \lambda(P_{\text{ref}} - P_0) \tag{8}$$

where P_{total} is the current magnitude for the load component; P_0 is the magnitude of this load component at the start of the step; P_{ref} is the magnitude of this load component as defined in the data for the step; and λ is the "load proportionality factor" that is found.

IV. Numerical Results and Correlation

A. Inflation

The first phase of the analysis, the inflation of the RCB, demonstrates that the rubber supports the majority of the inflation load as a membrane structure. The resultant stresses in the rubber are significantly less than needed to cause failure. The carbon fiber provides a radial stiffening, which develops the formation of a rigid rectangular cross-sectional structure as shown in Fig. 3.

B. Buckling Mode

In support of the experimental tests, the finite element analysis (FEA) results demonstrate that the RCB buckles predominantly in its first lateral buckling mode. This can be an expected mode of buckling for a slender beam subject to bending. In the analysis the

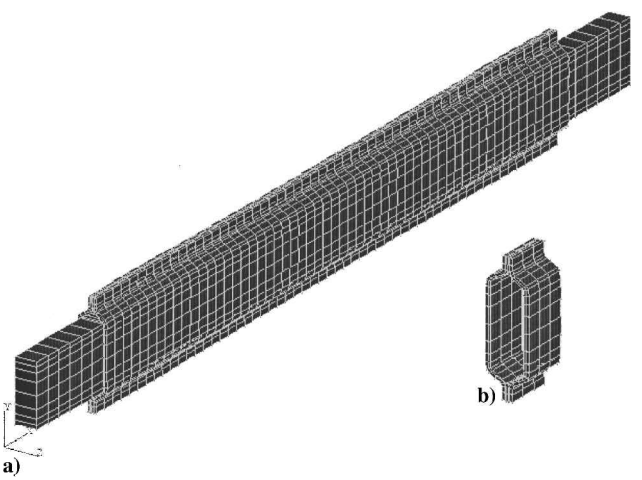

Fig. 3 Typical RCB: a) finite element solution for inflation and b) cross section of the middle.

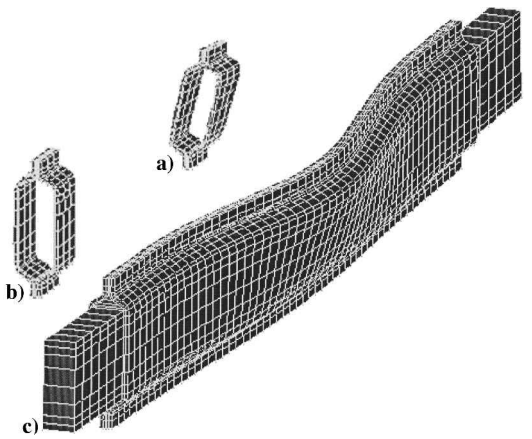

Fig. 4 Finite element result for the bending load case, depicting the a) middle section (buckled), b) end section (unbuckled) of the RCB, and c) distinct first lateral buckling mode for a typical RCB.

pneumatic cavity is free to deform with the structure. Its sole function is to transfer load to the carbon fiber composite in the form of air pressure. However, because of the enclosed pressurized air, the RCB is much stiffer in bending than an equivalent beam of comparable dimensions and material properties. The results obtained from the linear buckling analysis clearly support this statement. For the linear buckling analysis, the pressurized air is not included and thus does not contribute to stiffness. The lateral mode buckling predicted by the eigenvalue extraction is a very conservative estimate, because the analysis is a linear solution to what is a highly nonlinear problem. For example, the model's response is defined by its linear elastic stiffness in the base state (inflated shape), and the pneumatic properties are not included in the analysis. The results could thus represent the buckling of the inflated geometry without the stiffening effects of the air. In any respect this analysis will provide a conservative estimate of the buckling load for a range of RCB types solely for initial design purposes. The buckling load for this case is much reduced in magnitude, as can be seen from Table 3. Thus it is found that the buckling loads using the eigenvalue analysis method could provide preliminary conservative design estimates for the collapse load when the air pressure is not included.

This analysis is continued by performing an incremental load-deflection analysis, using the modified Rik method. Included in this analysis are all nonlinear effects such as material property, pneumatic stiffness, and preloaded inflation state to determine the nonlinear load-deflection response. Prior to the onset of buckling, the air supports the shape of the structure. In support of the experimental observations, the FEA has shown that as the center of the RCB starts to buckle in its lateral mode, the outer ends of the RCB (closest to the ends) begin to bulge as shown in Fig. 4. Once the RCB has started to buckle, the lateral and vertical displacements become, as expected, exceedingly large, and there is minimal resultant post-buckling stiffness. As compared to the linear eigenvalue results, the full nonlinear buckling loads listed in the second column of Table 3 agree favorably with the experimental results, more so for larger RCBs. The numerical prediction is within 8% of the experimental result for the largest RCB, S30, and 33% for the smallest RCB, S20. The increase in accuracy for larger RCBs may be attributed to the fabrication of the RCBs. In particular, the bonding of the plugs into each end of the RCBs may have led to the forming of excess adhesive in this region. The increase in adhesive would have the effect of stiffening the smaller RCB, S20. As the RCB size increases, the effect of this excess adhesive would be less compared to the relative size of the beam.

V. Conclusions

The primary aim of this work was the determination of the critical buckling load for a special case of a reinforced inflatable composite beam. In contrast to other types of inflatable structures, this special case has not been previously examined. A finite element and experimental study has been undertaken to examine this case carefully.

The following important observations have been made from the experimental and numerical results in this study. First, it has been demonstrated that air contributes significantly to the bending stability for this type of inflatable structure. Second, a full nonlinear finite element solution agrees favorably with experimental testing in bending. Third, a numerically efficient linear buckling solution provides a conservative design estimate of the maximum collapse load. Fourth, there is noticeable coupling between the pressurized air and the RCB at incipient collapse.

References

[1]Fichter, W. B., "A Theory for Inflated Thin-Wall Cylindrical Beams," NASA TN D-3466, 1966.

[2]Bulson, P. S., "Design Principles of Pneumatic Structures," *Structural Engineer*, Vol. 51, No. 6, 1973, pp. 209–215.

[3]Comer, R. L., and Levy, S., "Deflections of an Inflated Circular Cylindrical Cantilever Beam," *AIAA Journal*, Vol. 1, No. 7, 1963, pp. 1652–1655.

[4]Nowak, P. S., Sadeh, W. Z., and Jankus, J., "Feasibility Study of Inflatable Structures for a Lunar Base," *Journal of Spacecraft and Rockets*, Vol. 31, No. 3, 1994, pp. 453–457.

[5]Main, J. A., Peterson, S. W., and Strauss, A. M., "Load-Deflection Behavior of Space-Based Inflatable Fabric Beams," *Journal of Aerospace Engineering*, Vol. 7, No. 2, 1994, pp. 225–238.

[6]McComb, R. W., Zender, H. G., Jr., Shroud, G. W., and Leonard, W. J., "Analysis of Inflated Reentry and Space Structures," *Proceedings of the Recovery of Space Vehicles Symposium*, 1960.

[7]Leonard, R. W. H. G., Jr., Brooks, G. W., and McComb, H. G., Jr., "Structural Considerations of Inflatable Reentry Vehicles," NASA TN D-457, 1960.

[8]McComb, H. G., Jr., "A Linear Theory for Inflatable Plates of Arbitrary Shape," NASA TN D-930, 1961.

[9]Stroud, W. J., "Experimental and Theoretical Deflections and Natural Frequencies of an Inflatable Fabric Plate," NASA TN D-931, 1961.

[10]Topping, A. D., "Shear Deflections and Buckling Characteristics of Inflated Members," *Journal of Aircraft*, Vol. 1, No. 5, 1964, pp. 289–292.

[11]Stein, M., and Hedgepeth, J. M., "Analysis of Partly Wrinkled Membranes," NASA TN D-813, 1961.

[12]Darevskii, V. M., "Stability of a Console Cylindrical Shell under Bending by a Transverse Force with Twisting and Internal Pressure," *ARS Journal*, Vol. 31, 1961, pp. 125–133.

[13]Peterson, J. P., "Correlation of the Buckling Strength of Pressurized Cylinders in Compression or Bending with Structural Parameters," NASA TN D-526, 1960.

[14]Douglas, W. J., "Bending Stiffness of an Inflatable Cylindrical Cantilever Beam," *AIAA Journal*, Vol. 7, No. 7, 1969, pp. 1248–1253.

[15]Steeves, E. C., "A Linear Analysis of the Deformation of Pressure Stabilized Tubes," U.S. Army Natick Lab., Rept. NTIS N75-32513, 1975.

[16]Main, J. A., Peterson, S. W., and Strauss, A. M., "Beam-Type Bending of Space-Based Inflated Membrane Structures," *Journal of Aerospace Engineering*, Vol. 8, No. 2, 1995, pp. 120–128.

[17]Gosling, P. D., and Riches, C. G., "Some Results on the Load-Deflection Characteristics of Pneumatic Beams," *Proceedings IASS International Symposium on Shell and Spatial Structures*, Vol. 1, Nanyang Technological Univ., Singapore, 1997.

[18]Airtech Airpad Rubber, Airtech International, Carson, CA.

[19]Hexcel, Dublin, CA.

[20]ABAQUS Release Notes and Theory Manuals, Ver. 5.6. Hibbitt, Karlsonn and Sorensen, Pawtucket, RI, 1996.

[21]MSC/PATRAN Release Notes, Ver. 7. MacNeal–Schwendler, Los Angeles, 1996.

[22]Twizell, E. H., and Ogden, R. W., "Non-Linear Optimization of the Material Constants in Ogden's Stress-Deformation Function for Incompressible Isotropic Elastic Materials," *Journal of the Australian Mathematical Society Series B*, Vol. 24, 1983, pp. 424–434.

[23]Ogden, R. W., "Elastic Deformations of Rubberlike Solids," *Mechanics of Solids, The Rodney Hill 60th Anniversary Volume*, edited by H. G. Hopkins and M. J. Sewell, Permagon, New York, 1982.

[24]Knight, M., "Three Dimensional Elastic Moduli of Graphite/Epoxy Composites," *Journal of Composite Materials*, Vol. 16, 1982, pp. 153–159.

[25]Sandorf, P. E., "Transverse Shear Stiffness of T300/5208 Graphite-Epoxy in Simple Bending," Lockheed-California, Rept. LR29763, Burbank, CA, Nov. 30, 1981.

[26]Camponeschi, E. T., Jr., "Compression Response of Thick-Section Composite Materials," David Taylor Research Center Rept. DTRC SME-90-60, Annapolis, MD, Oct. 1990.

[27]MIL-HDBK-17-3E, DOD Coordination Working Draft, Vol. 3, Jan. 1997, Chap. 7, pp. 7-1–7-33.

E. R. Johnson
Associate Editor